3

Dental Biometrics for Human Identification

Aparecido Nilceu Marana[1], Elizabeth B. Barboza[2], João Paulo Papa[3], Michael Hofer[4] and Denise Tostes Oliveira[5]
[1,2,3]*Dept.of Computing, School of Sciences, São Paulo State University (UNESP), Bauru*
[4]*Institute of Medical Engineering, Graz University of Technology*
[5]*Bauru School of Dentistry, University of São Paulo (USP), Bauru*
[1,2,3,5]*Brazil*
[4]*Austria*

1. Introduction

In the history of civilization, the human identification based on dental information was first reported in the Roman Empire, when Nero's mother, Agripina, ordered the killing of Loilla Paulina, who was later identified by her dental caries and bad dental occlusion (Couto, 2009). The first treatise on human identification using dental records was conducted, in 1897, by Dr. Oscar Amoedo Valdés (1863-1945), a Cuban doctor, president of the French Dental Society and professor of the Paris Dental School, who applied a dental-based identification technique in order to reveal the identity of victims of a disaster which occurred in Paris (Amoedo, 1897).
Since Dr. Amoedo's work, the Forensic Dentistry has attracted much attention, and the importance of using dental records for human identification is nowadays accepted worldwide (Chen & Jain, 2005). During the last decade, dental records have been extensively used in order to identify the victims of massive disasters, such as the 9/11 terrorist attack in New York (O'Shaughnessy, 2002) and the tsunami in Asia (Thepgumpanat, 2005).
In Forensic Dentistry, the human experts perform manual comparisons of ante-mortem (AM) and post-mortem (PM) dental records, looking for similarities (Jain & Chen, 2004). During this manual approach, the main characteristics used to compare dental records are: the presence or absence of a specific tooth, the morphology and dental restoration of the teeth, periodontal tissue characteristics, pathologies and other anatomical features. Figure 1 shows panoramic radiographs of two distinct individuals. One can easily observe several differences between these radiographs. In contrast to other popular biometric characteristics, dental features do change over time, causing great difficulties during the identification task. The teeth can change in appearance as a result of dental restorations, or can be missing altogether due to an accident which occurred after the AM records were taken. For this reason, although accepted in courts of law, dental based identification is considered less reliable than other biometric methods (Jain et al., 2003). Figure 2 shows panoramic radiographs of the same individual taken at two separate occasions during a period of three years. The dental patterns are almost the same, but changes due to dental restorations can be observed.
Despite known drawbacks of these identification methods, dental information may be the only available mean for identification in many disaster scenarios and mass accidents like fire and plane crashes. The other popular methods of identification are impossible since physical traits like faces and fingerprints are, in general, completely destroyed in such events

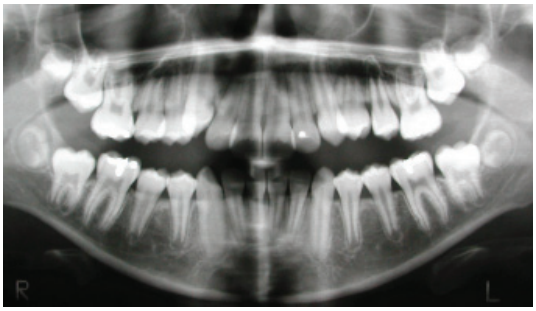

(a)

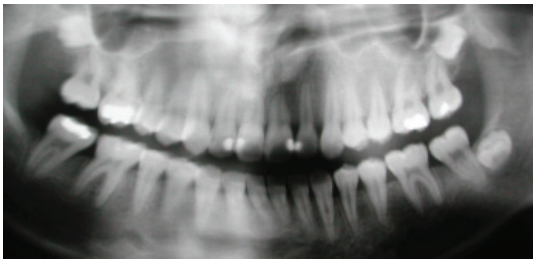

(b)

Fig. 1. Panoramic radiographs of two distinct adult individuals. It is possible to observe several details in teeth patterns that can be used to distinguish the individuals by their dental radiographs.

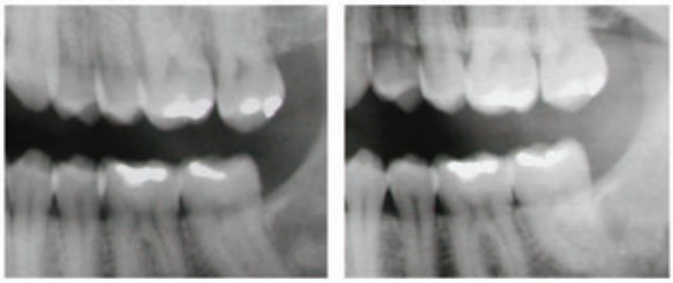

Fig. 2. Panoramic radiographs of the same person. (a) Acquired in the year 2000; (b) Acquired in the year 2003.

(Tang et al., 2009). The teeth and their dental restorations are very resistant to modest force effects and high temperatures. The teeth need a high temperature to be annealed and the components of the dental restorations likewise have a very high melting point. Savio et al. (2006) carried out an in-vitro experiment where, after exposing teeth to fire, periapical radiographs of all the teeth were taken. They reported a number of significant radiographic characteristics of the teeth were conserved after the exposure: the composite fillings were in place maintaining the shape up to $600^{o}C$ ($1112^{o}F$), the amalgam fillings were in

place maintaining the shape up to 1000^oC (1832^oF) and the endodontic treatments were recognizable up to 1100^oC (2012^oF).
Even when the person has never undergone dental treatment, the Forensic Dentistry can provide additional important information for the identification of the victim, such as species, racial group, gender, age, height, possible profession, and other private information which can facilitate police investigations.
When adult dentition is complete, dental-based identification process can provide high recognition rates, since no two individuals share the same teeth structure and characteristics. However, despite its accuracy, the traditional manual dental records comparison method demands too much time, and is not applicable in large scale identification, like mass disasters. Therefore, the development of techniques and systems that facilitate human identification through automated teeth recognition has become a necessity.
>From the Pattern Recognition and Computer Vision point of view, the problem of person identification based on dental records can be defined as an image matching and retrieval problem. That is, given an input dental image (usually a PM radiograph), the system searches the database in order to find the best matching AM radiograph (Jain et al., 2003).
The goal of this chapter is to introduce the problem of human identification based on dental biometrics, to summarize several techniques proposed in the specialized literature for automated dental recognition, to describe in detail an original method for dental recognition based on a new biometric descriptor, called dental code, and to propose a new method for dental recognition using the Image-Foresting Transform (Falcao et al., 2004) and the Shape Context (Belongie et al., 2000).

2. Automated Dental Identification Systems

Recent mass disasters, like the 9/11 terrorist attack and the Asian Tsunami, have highlighted the significance of automated dental identification systems (ADIS). In both these disasters, many victims were identified only by parts of their jaw bones. In the Asian tsunami, for instance, about 75% of the victims were identified using dental records, compared to just 0,5% victims which were identified using DNA (NewScientists, 2005). However, since the method of manual identification was used, it took several months to identify only a small part of the victim groups (only 20% of the 9/11 attack victims were identified in the first 12 months, and only 1,15% of the Asian tsunami victims were identified in the first 9 months). Therefore, we can conclude that manual dental identification is a very efficient post-mortem identification tool, but is also a time consuming process.
Besides being a humanitarian issue, a fast and precise post-mortem human identification is also is crucial in solving problems related to heritage, proprietorship, insurance policies, pension charging, etc. Thus, the development of Automated Dental Identification Systems (ADIS) is a necessity. Automating dental identification methods will enhance the process of human identification in catastrophic events where the use of biometric identifiers such as face and fingerprints may not be possible (Abaza et al., 2009).
According to Fahmy et al. (2004), a typical architecture of an ADIS is composed of three main components: dental record preprocessing, search and retrieval, and image comparison. Figure 3 illustrates main phases of a person identification system based on dental records. In the first phase, the query radiograph is preprocessed in order to enhance its contrast, remove its noises, and select the areas of interest. The segmentation of the teeth and the normalization of the image regarding discrepancies in scale, rotation and illumination are also carried out at this stage. Next, a template (or model) image is retrieved from the database and is registered with the query image, for matching. In the following, decision making phase, the features

extracted from the teeth on both images are compared by using a proper distance function. The system output is, in general, a score proportional to the probability of both radiograph images being of the same individual.

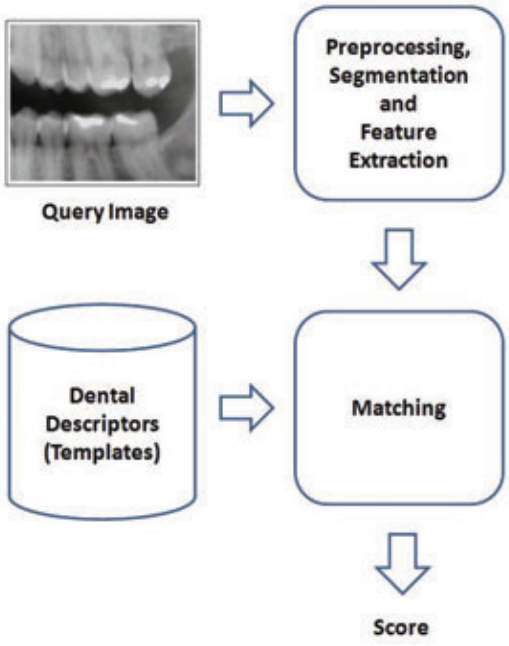

Fig. 3. Typical ADIS components.

Chen & Jain (2005) proposed an ADIS that has two main stages: feature extraction and matching. The feature extraction stage uses anisotropic diffusion to enhance the images and a Mixture of Gaussians model to segment the dental restorations. The matching stage has three sequential steps: tooth-level matching, computation of image distances, and subject identification. In the tooth-level matching step, tooth contours are matched using a shape registration method, and the dental restorations are matched on overlapping areas. The distance between the tooth contours and the distance between the dental restorations are then combined using posterior probabilities. In the second step, the tooth correspondences between the given query (post-mortem) radiograph and the database (ante-mortem) radiograph are established. A distance based on the corresponding teeth is then used to measure the similarity between the two radiographs. Finally, all the distances between the given post-mortem radiographs and the ante-mortem radiographs that provide candidate identities are combined to establish the identity of the subject associated with the post-mortem radiographs.

Zhou & Abdel-Mottaleb (2005) presented a system to assist human identification using dental radiographs. The goal of their system is to archive ante-mortem (AM) dental images and enable content-based retrieval of AM images that have similar teeth shapes to a given post-mortem (PM) dental image. During archiving, the system classifies the dental images to bitewing, periapical, and panoramic views. It then segments the teeth and the bones in the bitewing images, separates each tooth into the crown and the root, and stores the contours

of the teeth in the database. During retrieval, the proposed system retrieves from the AM database the images with the teeth most similar to the PM image based on Hausdorff distance measure between the teeth contours.
Abaza et al. (2009) considered archiving and retrieving dental records from large databases to be a challenging task which has not received adequate attention in the literature. Therefore, they propose an efficient method for retrieving dental records from a database in order to assist the forensic expert in identifying deceased individuals in a rapid manner. The proposed method is an appearance-based technique that consolidates the evidence presented by individual teeth in a dental record, that is, it moves from tooth-to-tooth in order to render a record-to-record matching score. The proposed method is shown to reduce the searching time of record-to-record matching by a factor of a hundred.
Hofer & Marana (2007) proposed a method for human identification based on dental restorations observed in panoramic radiographs. The proposed method has three main processing steps: automatic segmentation of dental restorations, creation of a dental code, and matching. In the segmentation step, seed points of the dental restorations are detected by thresholding. The final segmentation is obtained with a snake (active contour) algorithm. The dental code is defined from the location and size of the dental restorations, and the distance between them. The matching stage is performed with the generalized edit distance (Levenshtein distance) (Navarro, 2001). Details of this method are presented next.

3. Proposed method for human identification based on dental restorations information

The new method proposed by Hofer & Marana (2007) for human identification based on dental restorations consists of three main steps: preprocessing of the dental radiographs and segmentation of the dental restorations (DRs); creation of a dental code (DC) out of the information of the detected DRs including the size, the location and the distance between them; and matching of a query DC with a template DC taken from the database.

3.1 Preprocessing and Segmentation

The dental radiograph image (RGB image) is converted into a gray-scale image and a median filtering is performed to reduce noise. Because of different contrast conditions in the dental radiographs, the image is subdivided into 2 regions of interest (ROIs), as illustrated in Figure 4.

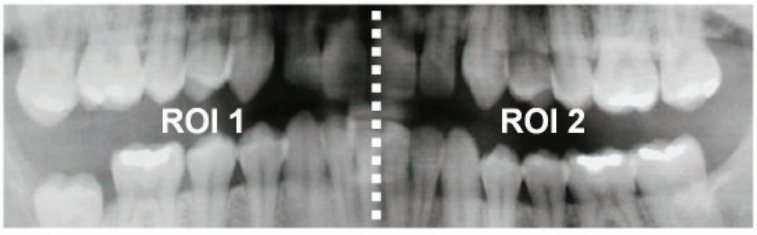

Fig. 4. ROIs in a dental radiograph, left part (ROI 1), right part (ROI 2).

The algorithm determines a gray value threshold in the left and in the right ROIs of the dental radiograph. Typically, the DRs feature the highest intensities in the image and appear as a distinct, relatively small but pronounced mode in the upper range of the gray-scale histogram. After smoothing the histogram with a moving average filter, the threshold is set

to the gray-value at the location of the left valley at the rightmost mode, which indicates the DRs, as shown in Figure 5.

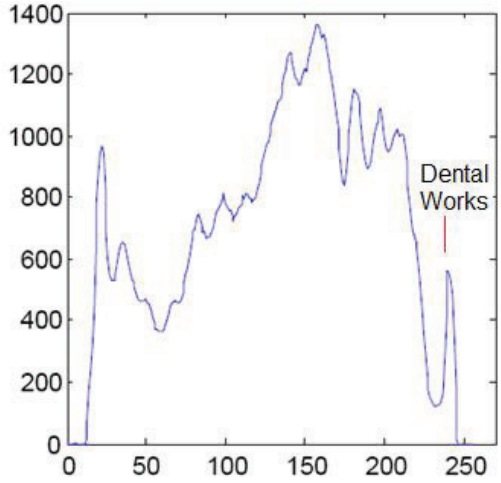

Fig. 5. Smoothed histogram of the ROI 2 in Figure 4 (threshold value is 232).

The threshold value is used to binarize the gray-level image. The results of the conversion are used to initialize the contour for the segmentation method. Each region represents a possible DR.

A snake (active contour) algorithm, as defined by Xu & Prince (1998), is used to perform the final segmentation of the DRs. Snakes can be used to segment objects with fuzzy border contours where traditional edge-detection (Ziou & Tabbone, 1998) will fail. Snakes are curves that can move under the influence of internal forces (elasticity and bending forces) coming from within the curve itself, and external forces (potential forces) computed from the image data. The internal and external forces are defined so that the final snake will conform to an object boundary (Xu & Prince, 1998). The external force field is computed from the gradient image. A snake needs to be initialized with an initial curve (e.g. circle) and is an iterative procedure which stops after a defined number of iterations. The better the initialization curve, the better the performance of the algorithm and the final segmentation results.

Each DR is segmented with a separate snake. To improve the segmentation and to speed up the algorithm, the initial curves for all DRs are computed from the binary mask. The borders of the detected regions are used as initial curves. The evaluation of the snake is shown in Figure 6.

Finally, a binary mask of the image including all detected DRs is created. This mask is called a dental restorations mask (DRM).

3.2 Creation of the Dental Code

Based on the DRM, a dental code (DC) is created. The DC incorporates information about the location, the size of the DRs and the distance between two DRs next to each other.

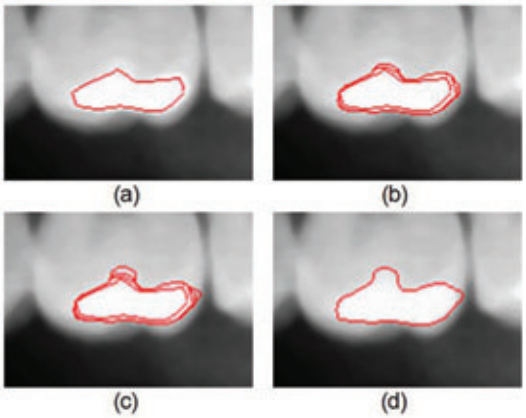

Fig. 6. Segmentation process. (a) Initial curve; (b) Curve transformation after 2 iterations; (c) After 5 iterations; (d) Final segmentation result after 30 iterations.

3.2.1 Locations of the dental restorations

An algorithm was implemented to sort all DRs into the DRM moving from left to right, based on the leftmost pixel of each individual DR, as illustrated in Figure 7.

Fig. 7. Dental restorations mask with sorted dental restorations from left to right.

An important factor for the creation of the DC is whether the tooth on which the DR is located belongs to the upper or to the lower jaw. Therefore, a border between the upper and the lower row of teeth has to be defined. A stripe in the intensity image is cut with the width of the current region. Next, the intensity sum of all horizontal rows in the stripe is calculated. The highest intensity represents the area of the DR, as illustrated in Figure 8.
The algorithm detects the first valley on the left and on the right side of the highest intensity point. The valley with the lower intensity represents the border between the upper and the lower row of teeth. If the position of this valley is above the DR in the image, the DR belongs to the lower row of teeth. If the position is below the DR, the DR belongs to the upper row of teeth. The locations of the dental restorations are represented in the DC with the letter "L" or "U" (Letter "L": DR on the lower row of teeth, Letter "U": DR on the upper row of teeth).

3.2.2 Size of the dental restorations

The proposed method uses registered dental radiographs images which are all resized to be the same size. Consequently, the amount of pixels in a dental radiograph is always the same, which means that the size of a DR (amount of pixels) is a percentage of the total amount of pixels in the dental radiograph.

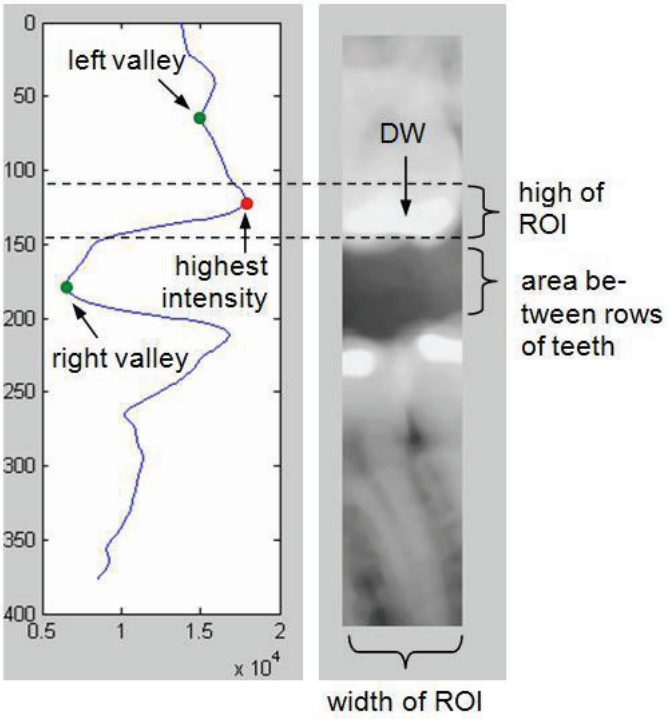

Fig. 8. Cut stripe and sum of intensities; right valley represents lower intensity which indicated that the DR belongs to the upper row of teeth, (dental code = "U").

3.2.3 Distance between two dental restorations

To make the matching algorithm more sensitive, the distance (amount of pixels) between the center of the mass point of a DR and its left neighbor is also included in the DC, as illustrated in Figure 9. The distance of the leftmost DR is set to zero. The value for the distance is given in percentage of the total width of the dental radiograph.

Fig. 9. Distances between dental restorations.

The DC is created out of this information as follows: 1) the position of the DR ("L" or "U"); 2) the size of the DR; 3) the distance between the current DR and the previous DR (from left to right). An example of a finalized DC for a panoramic dental radiograph is shown in Figure 10.

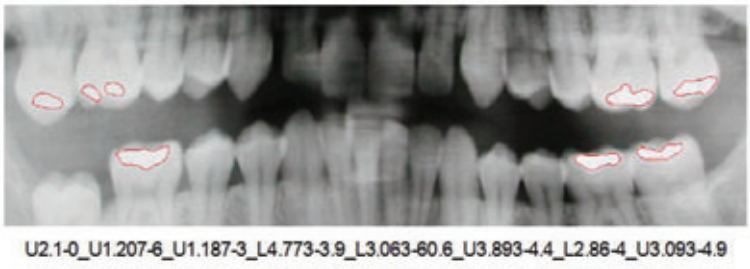

Fig. 10. Dental code (DC) obtained from a panoramic dental radiograph.

3.3 Matching

After the DC is created, it can be compared to other DCs in a database. These can be different codes of the same person, due to possible changes in dental restorations, as illustrated in Figure 2, or codes of different subjects. Matching between radiographs of the same subject is called "genuine matching" and matching between radiographs belonging to two different subjects is called "impostor matching". An algorithm was implemented based on the generalized edit distance (Levenshtein distance). The edit distance between two strings is given by the minimum number of operations needed to transform one string into the other, where an operation is an insertion, a deletion, or a substitution (Navarro, 2001).

In the edit distance, every edit operation is associated with certain costs. For instance, to transform the string *hitten* into *sitting*, it is necessary to substitute 'h' for 's', 'e' for 'i', and finally, to insert 'g' at the end. The overall Edit distance cost in this example is 3, using the same cost for each operation. It is also possible to change the cost of different operations (insertion, deletion, or substitution).

The edit distance has received a lot of attention because its generalized version is powerful enough for a wide range of applications (Navarro, 2001).

Because of the structure of the DC, it was necessary to adjust the edit distance costs. Not only the letters "U" and "L" have to be compared, but also the size of the DRs and the distance between two DRs. The costs of the insertion, deletion, and substitution were changed to improve the results of the matching algorithm. In the case of insertion and deletion, the matching cost is 60 (see Table 1). In the case of substitution the cost for comparing two DRs is given by the sum of two costs: the cost of comparing the size, and the cost of comparing the distance between two DRs. If the compared sizes differ more the 100%, the cost is set to 25. Otherwise, the cost for comparing the size is set according to the percentage difference of the two compared DRs (see Table 1). If the compared distances differ more than 15%, the cost is set to 25. Otherwise, the cost for comparing the distances is set according to the percentage difference of compared DRs (see Table 1).

3.4 Assessment of the proposed method

In order to assess the proposed dental biometric method, some experiments were carried out on a database including 68 panoramic dental radiographs: a pair of panoramic radiographs for each of 22 adult subjects (44 panoramic radiographs) plus a single panoramic radiograph

Operation	Cost
Insertion	60
Deletion	60
Substitution Comparing Size	0, difference between 0 . . . 10% 1, difference between 10 . . . 20% ⋮ 10, difference between 90 . . . 100% 25, difference > 100%
Substitution Comparing Distances	0, difference between 0 . . . 1% 1, difference between 1 . . . 2% ⋮ 15, difference between 14 . . . 15% 25, difference > 15%

Table 1. Edit distance costs for insertion, deletion and substitution.

for each of other 24 subjects. For the purpose of the study, the older radiographs of the 22 subjects with two panoramic radiographs were considered AM (ante-mortem) while their newer radiographs were considered PM (post-mortem). The radiographs of the 24 subjects with only one panoramic radiograph were considered AM.

In the experiments, the images were manually registered to obtain comparable conditions. In cases of over-segmentation or under-segmentation of the DRs, the segmentation results were manually corrected. Likewise, if a DR could not be detected by thresholding, a ROI was manually selected in the radiograph to perform local thresholding. Segmentation results and their corresponding DCs for two panoramic radiographs are shown in Figure 11.

In order to test the matching performance of the method, an algorithm was implemented to compare panoramic radiographs of the genuine class (two radiographs of the same person) and panoramic radiographs of the impostor class (two radiographs of different persons). Figure 12(a) shows a receiver operating characteristic (ROC) curve, which plots the false acceptance rate (FAR) versus the false rejection rate (FRR) for different threshold values. The ROC curve shows that the proposed method obtained 11% of equal error rate (EER) for the used database, which is a good result. The equal error rate (EER) is the value where the FAR is equal to the FRR. The lower the EER, the better the performance of the biometric system. Figure 12(b) shows the accuracy curve obtained when the 22 PM radiographs were matched to the 46 AM radiographs from the database. Using the top-1 retrieval, the accuracy was 19/22 (= 86%). Using top-8 retrievals, the retrieving accuracy was 95%. The accuracy reached 100% when the top-11 retrievals were used.

4. Dental recognition based on image-foresting transform and shape context

The assessment of the proposed method for human identification based on dental restorations information (Section 3) brought us to a conclusion that the segmentation step is crucial. Based on the good results obtained by Falguera et al. (2008), who used other biometrics characteristics from radiographs, such as the frontal sinus, we opted to use the Differential Image-Foresting Transform (DIFT), proposed by Falcao & Bergo (2004), for dental segmentation. The main idea is to design an interactive ADIS, where the user has to indicate only a few points (seeds) inside and outside of the dental restorations.

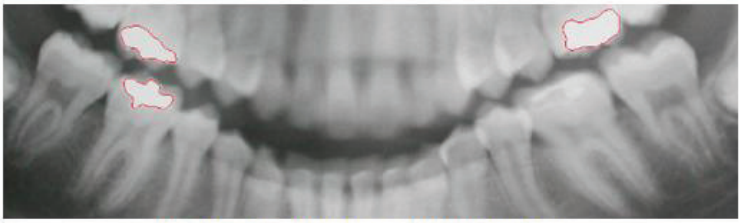

DC=U6.997-19.5_L6.147-0.1_U9.523-60_

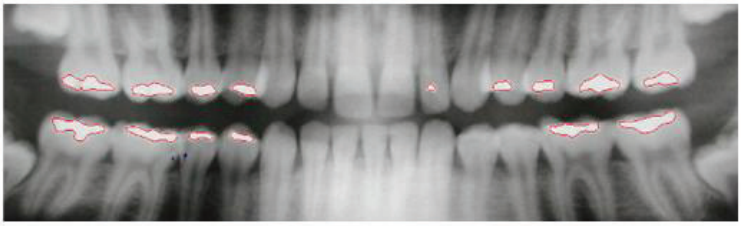

DC=L3.877-10.1_U3.357-1.2_U2.543-8.9_L2.57-0.1_L0.947-6.5_U1.453-0.5_L0.953-5.1_U1.233-0.5_U0.273-25.2_U0.937-9.7_U1.287-5.6_L2.67-4.1_U2.927-3.5_L3.733-6.8_U1.913-1.6_

Fig. 11. Segmentation results of two dental radiographs including their dental codes.

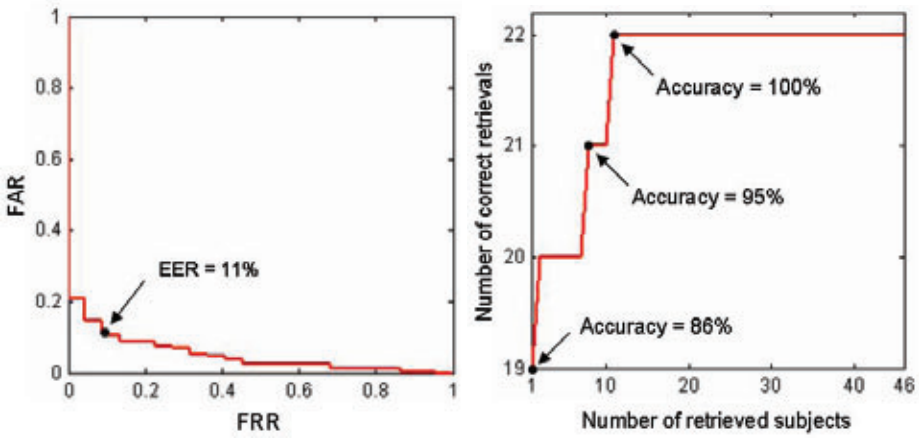

(a) ROC Curve: EER=9.8%. (b) CMC Curve: CRR = 100% at Top 11.

Fig. 12. Results obtained with the proposed method based on dental restorations recognition.

Figure 13 presents the dental restorations segmentation obtained from a panoramic radiograph using the DIFT-based segmentation algorithm. One can observe that the algorithm obtained very good dental restorations segmentations with minimal user intervention using only a few external (white spots) and internal seeds (yellow spots).
Also, in order to improve the recognition rates, we propose the fusion of the dental restorations based method with a more precise method based on teeth shapes segmented

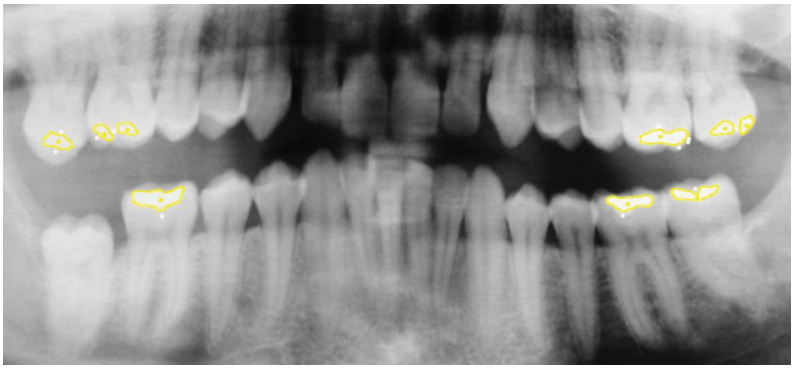

Fig. 13. Automated dental restorations segmentation using the DIFT-based segmentation algorithm. White spots: external seeds. Yellow spots: internal seeds.

in the panoramic radiograph. In this multibiometrics method, we compute the query and template radiographs matching score as a weighted sum of dental restorations matching score and the teeth shapes matching score. The teeth shapes matching score is computed by using the shape context method, proposed by Belongie et al. (2000).
Figure 14 shows the interface of our interactive ADIS, during the matching stage, in which the shape of a molar tooth from the query radiograph is being compared with the shape of the same molar tooth, but from a template radiograph.

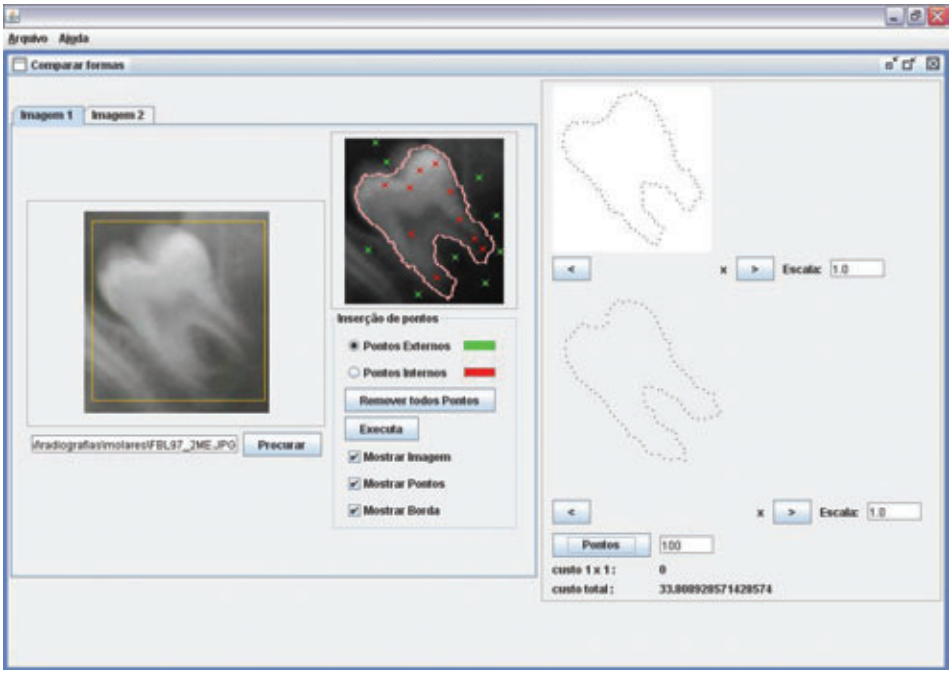

Fig. 14. Proposed ADIS (Automated Dental Identification System) for dental recognition.

In the following sections, the DIFT and the Shape Context methods for segmentation and shape comparison are summarized respectively.

4.1 Differential image-foresting transform segmentation method

The image segmentation algorithm based on Differential Image Foresting Transform (DIFT) was proposed by Falcao & Bergo (2004). This algorithm reduces the image segmentation problem to the calculation of minimum cost path forests in the graph derived from the image. The search for minimum cost paths is restricted to paths that have origin in a set of initial pixels called seeds.

The function that determines the cost of the path between two nodes of the graph is the difference between the gray levels of the pixels that are represented by graph nodes. This way, pixels with similar gray levels will have smaller path costs and will tend to be connected to each other, originating plateaus in the image.

Therefore, using this algorithm, the human intervention during the image segmentation is reduced to the choice of a few seeds (pixels) inside and outside of the object to be segmented. Then, the seeds will compete for the graph nodes in each interaction, creating, in the end, internal and external regions related to the object of interest, in which the terminal pixels delimitate the object (Miranda, 2006).

Figure 15(a) presents a graph of a gray level two-dimensional image, in a 4-neighborhood system. The numbers correspond to the intensities $I(p)$ of the pixels and the biggest circles represent two seeds: one inside and the other outside the object which is to be segmented (in this example, a rectangle in the center of the image) (Miranda, 2006).

Figure 15(b) shows the minimum cost path forest, obtained using the cost function $C(p,q) = |I(q) - I(p)|$, where $I(p)$ is the intensity of a pixel and $I(q)$ is the intensity of the preceding pixel. The shown numbers are the values of the calculated costs. The segmentation of the rectangle at the center of the image is obtained by the tree rooted in the internal seed. The arrows points to the predecessor of each node in the optimum path (Miranda, 2006).

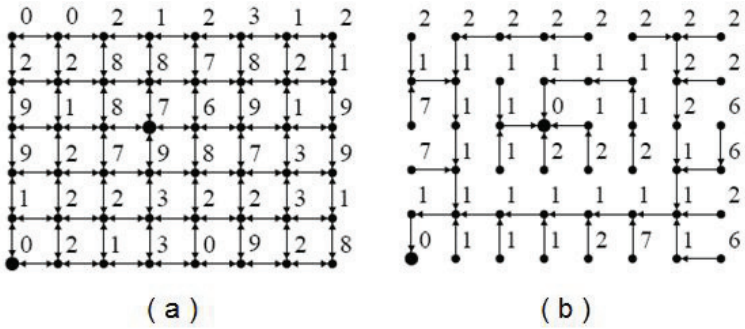

Fig. 15. (a) Graph of a gray level 2D image in a 4-neighborhood. (b) Minimum cost path forest obtained for the graph under (a) (Miranda, 2006).

In case of a non-satisfactory segmentation, the user can add more inside or outside seeds and re-run the algorithm. Instead of calculating a new minimum cost path forest every time the seed set is changed, the DIFT-based segmentation algorithm only updates the segmentation result in a differential way, within a time frame proportional to the number of nodes inside the changed regions of the forest, reducing the execution period up to ten times compared to the original IFT-based segmentation algorithm, proposed in (Miranda, 2006).

4.2 Shape context description method

Shape Context is a method for shape description proposed by Belongie et al. (2000). This description method calculates the polar-logarithmic distribution of shape border points in relation to a certain point p, which belongs to the shape border. This provides a global and discriminative characterization of the shape. Thus, the corresponding border points of two similar shapes will have similar shape contexts. The similarity measurement between two objects is computed as being the minimum cost of alignment among the border points of their shapes. The more different the shapes of the objects, the greater their alignment cost.
Figure 16(a) presents the polar-logarithmic histogram representation used to calculate the shape context for each point of the shape border in respect to the other points. In this example, the histogram is composed by 60 bins (12 angles and 5 distances). Figure 16(b) shows the polar-logarithmic histogram obtained for the border point of the shape selected in the Figure 16(a).

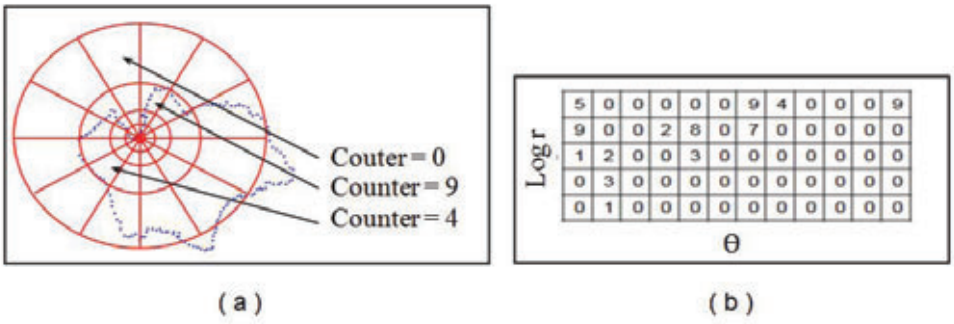

Fig. 16. (a) Illustration of the log-polar histogram computation for one shape; (b) Shape context histogram computed for the shape point shown in (a).

Figure 17 illustrates a comparison between histograms of three distinct points of two shapes. One can note that the two points located at similar regions (top-left) of the border present similar histograms. On the other hand, the third point, located at a different location (bottom-right) presents a very different histogram. To make the visualization easier, the values of the histograms were mapped into gray levels: the darker the position at the histogram, the greater the occurrence of border points at that angle and distance.
The similarity between two shapes is computed as the minimum cost of alignment obtained for them, using the shape context descriptors for every pixel belonging to each shape. The smaller the cost, the larger the similarity score between the shapes. Given the pixels p_i and p_j, belonging to each border shape that are being compared, once the shape contexts of each pixel are distributions represented by histograms, it is possible to utilize the statistic test χ^2, given by equation 1, to calculate the matching cost C_{ij} between p_i and p_j, where $h_i(k)$ and $h_j(k)$ denote the normalized histograms of p_i and p_j, respectively, and K represents the number of histogram bins.

$$C_{ij} = \frac{1}{2}\sum_{k=1}^{K}\frac{[h_i(k) - h_j(k)]^2}{h_i(k) + h_j(k)} \tag{1}$$

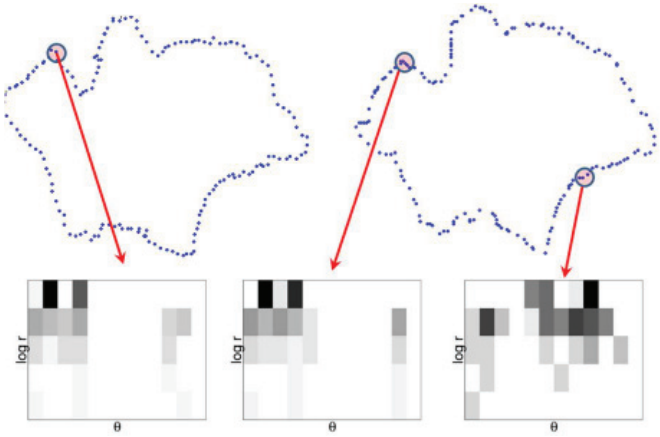

Fig. 17. Comparison of histograms of three distinct points on two shapes obtained from the same source.

5. Conclusion

In Forensic Dentistry, human experts generally perform manual comparisons of ante-mortem and post-mortem dental records, looking for differences among teeth patterns. Despite its accuracy, this manual comparison method demands great amount of time, which is not admissible in large scale identification. Therefore, the development of techniques and systems that facilitate human identification through automated teeth recognition is required.

In the last years, some ADIS (Automated Dental Identification Systems) have been proposed in the literature. In our research in this area, we have proposed an ADIS based on dental restorations recognition and teeth shapes analysis. The results obtained with the dental restorations features can be considered good, when the high variability of this biometric characteristic is observed. To cope with this high variability, we proposed a very promising distance function based on the generalized edit distance.

In order to improve the recognition rates, we also proposed the fusion of a teeth restorations based method and a teeth shapes based method, in which the teeth shapes are extracted from panoramic radiographs images using a Differential Image-Foresting Transform (DIFT) segmentation algorithm and the shape analysis is carried out using the Shape Context method. The DIFT segmentation algorithm and the Shape Context method were employed by the authors for another kind of biometrics trait, the frontal sinus, providing very good results. The same good performance level is expected to be reached in the application of these methods on panoramic dental radiographs. Results obtained from the fusion with both methods will be published soon.

6. References

Abaza, A., Ross, A. & Ammar, H. (2009). Retrieving dental radiographs for postmortem identification, *Proc. of IEEE International Conference on Image Processing (ICIP)*.

Amoedo, O. (1897). The role of the dentists in the identification of the victims of the catastrophe of the 'bazar de la charité', paris, 4th of may,1897, *The Dental Cosmos* 39: 905–12.

Belongie, S., Malik, J. & Puzicha, J. (2000). Shape context: A new descriptor for shape matching and object recognition, *Neural Information Processing Systems Conference (NIPS)*, pp. 831–837.

Chen, H. & Jain, A. K. (2005). Dental biometrics: Alignment and matching of dental radiographs, *IEEE Trans. Pattern Anal. Mach. Intell.* 27(8): 1319–1326.

Couto, M. I. S. B. G. (2009). *Importância dos Registros Dentários em Situações de Grandes Catástrofes*, Master Dissertation in Forensic Medicine, Instituto de Ciências Biomédicas Abel Salazar, Universidade do Porto, Portugal.

Fahmy, G., Nassar, D., Haj-Said, E., Chen, H., Nomir, O., Zhou, J., Howell, R., Ammar, H. H., Abdel-Mottaleb, M. & Jain, A. K. (2004). Towards an automated dental identification system (adis), *in* D. Zhang & A. K. Jain (eds), *Biometric Authentication*, Vol. 3072 of *Lecture Notes in Computer Science*, Springer Berlin / Heidelberg, pp. 1–41.

Falcao, A., Stolfi, J. & de Alencar Lotufo, R. (2004). The image foresting transform: theory, algorithms, and applications, *Pattern Analysis and Machine Intelligence, IEEE Transactions on* 26(1): 19 – 29.

Falcao, A. X. & Bergo, F. P. G. (2004). Interactive volume segmentation with differential image foresting transforms, *IEEE Trans. on Medical Imaging* 23(9): 1100–1108.

Falguera, J. R., Falguera, F. P. S. & Marana, A. N. (2008). Frontal sinus recognition for human identification, SPIE, p. 69440S.

Hofer, M. & Marana, A. N. (2007). Dental biometrics: Human identification based on dental work information, *Proc. XX Brazilian Symposium on Computer Graphics and Image Processing, 2007 (SIBGRAPI 2007).*, pp. 281 –286.

Jain, A. K. & Chen, H. S. (2004). Tooth contour extraction for matching dental radiographs, *Proc. 17th ICPR, vol. III*, Cambridge, UK, pp. 522–525.

Jain, A. K., Chen, H. S. & Minut, S. (2003). Dental biometrics: Human identification using dental radiographs, *Proc. 4th Int. Conf. on Audio and Video-Based Biometric Person Authentication (AVBPA)*, Guildford, UK, pp. 429–437.

Miranda, P. A. V. (2006). *Segmentação de Imagens pela Transformada Imagem-Floresta*, Master Dissertation, Institute of Computing, UNICAMP, Campinas, Brazil.

Navarro, G. (2001). A guided tour to approximate string matching, *ACM Comput. Surveys* 33(1): 31–88.

NewScientists (2005). Dental records beat dna in tsunami ids.
URL: *NewScientists.com News Service*

O'Shaughnessy, P. (2002). More than half of victims idd, *New York Daily News* .

Savio, C., Merlati, G., Danesino, P., Fassina, G. & Menghini, P. (2006). Radiographic evaluation of teeth subjected to high temperatures: Experimental study to aid identification processes, *Forensic Science International* 158(2): 108–116.

Tang, J. P., Hu, D. Y., Jiang, F. H. & Yu, X. (2009). Assessing forensic applications of the frontal sinus in a chinese han population, *Forensic Science International* 183(1-3): 104.e1 – 104.e3.

Thepgumpanat, P. (2005). Thai tsunami forensic centre produces first ids, *Reuters* .
URL: *http://www.alertnet.org/*

Xu, C. & Prince, J. L. (1998). Snakes, shapes, and gradient vector flow, *IEEE Transactions on Image Processing* 7(3): 359–369.

Zhou, J. & Abdel-Mottaleb, M. (2005). A content-based system for human identification based on bitewing dental x-ray images, *Pattern Recognition* 38(11): 2132 – 2142.

Ziou, D. & Tabbone, S. (1998). Edge detection techniques - an overview, *International Journal of Pattern Recognition and Image Analysis* 8: 537–559.